INORGANIC CHEMISTRY
FRONTIERS

RESEARCH ARTICLE

View Article Online
View Journal

Check for updates

Cite this: DOI: 10.1039/d5qi02464a

Al pairing in 8-membered rings drives superior methanol amination on CHA zeolites

Shuang Liu,[a] Pan Xu,[a] Sihui Li,[a] Junyao Pan,[a] Yuxin Yan,[a] Rui Wu,[b] Junhui Guo,[c] Chang Liu*[c] and Wenfu Yan *[a]

In protonic acid-catalyzed methanol amination, achieving high selectivity toward methylamine (MMA) and dimethylamine (DMA) while suppressing dimethyl ether (DME) formation remains challenging. The catalytic performance of protonic zeolites in this reaction depends on Brønsted acidity, which is controlled by both the Si/Al ratio and the spatial distribution of framework Al. **CHA** zeolite is particularly attractive because of its unique pore architecture and tunable acidity. Here, we synthesized **CHA** zeolites with Si/Al ratios from 3.4 to 4.3 and systematically varied their Al distributions, without using organic structure-directing agents (OSDAs). The synthesis exploited the synergistic effect of alkali metal cations (Na^+, Cs^+) and **CHA** seeds with different Al contents (SAPO-34, SSZ-13, and pure silica **CHA**). The Al content of the seed determined the Si/Al ratio of the final product, while the seed type controlled the Al distribution. At a fixed Si/Al ratio of 3.8, the sample synthesized with a SAPO-34 seed (CHA-S34-3.8) showed the best performance. At 350 °C and 0.813 h^{-1}, and at 400 °C and 4.3 h^{-1}, MMA + DMA yield reached 86.6% and 87.6%, respectively, with no detectable DME after stabilization. These values represent the highest reported performance for methanol amination. Characterization revealed that enrichment of Al pairs in the eight-membered rings, combined with optimal acid density and strength, accounts for the superior activity. This study provides mechanistic insight into the role of Al distribution and offers a strategy to design high-performance zeolite catalysts for methanol amination.

Received 5th December 2025,
Accepted 16th January 2026

DOI: 10.1039/d5qi02464a

rsc.li/frontiers-inorganic

Open Access Article. Published on 19 January 2026. Downloaded on 2/25/2026 1:52:34 AM.
This article is licensed under a Creative Commons Attribution-NonCommercial 3.0 Unported Licence.

1. Introduction

Monomethylamine (MMA, 3.7 × 3.9 × 4.4 Å), dimethylamine (DMA, 3.9 × 4.7 × 6.0 Å), and trimethylamine (TMA, 3.9 × 5.4 × 6.1 Å) are important intermediates in the production of solvents, agrochemicals, surfactants, and water treatment agents.[1,2] Industrially, these amines are produced by reacting methanol with ammonia. However, the reaction thermodynamically favors TMA, even though market demand is greater for MMA and DMA.[3,4] Improving selectivity toward MMA and DMA is therefore essential to reduce both energy consumption and downstream separation costs.

Early catalysts, including γ-Al_2O_3 and amorphous silica–alumina, favored TMA formation and produced significant amounts of dimethyl ether (DME) as a by-product.[3] To overcome these drawbacks, research has focused on developing catalysts that enhance MMA and DMA selectivity while suppressing side reactions. Zeolites are particularly attractive because of their ordered porosity, high surface area, and tunable Brønsted acidity.[5,6] Modified mordenite (**MOR**) was the first commercial zeolite catalyst used for methanol amination in the 1980s. However, its 12-membered ring (12MR, ~6.5 × 7.0 Å) channels are too large to restrict the diffusion and formation of TMA.[7] This limitation shifted attention toward smaller-pore zeolites.

Zeolites with eight-membered rings (8MR, 3.0–4.5 Å) are especially promising because their pore sizes closely match those of low-substituted amines. Representative 8MR frameworks include **LEV**, **MTF**, **DDR**, **UFI**, **CHA**, **AFX**, **PWN**, **RHO**, **PAU**, **KFI**, and **LTA**.[1,8–13] Their performance in methanol amination depends on both shape selectivity and Brønsted acidity. A high density of acid sites accelerates methanol conversion but also promotes over-methylation to TMA. Strongly methylated ammonium ions can also block pores, which in turn suppresses DME formation.[9] Acid strength plays an equally critical role: excessively strong acidity favors TMA and DME formation, while weak acidity destabilizes methylammonium intermediates, also leading to DME. Moderate acidity strikes the right balance, favoring MMA and DMA production.[3,7,8] In addition, the spatial distribution of acid sites strongly influences product selectivity.[3]

[a]State Key Laboratory of Inorganic Synthesis and Preparative Chemistry, College of Chemistry, Jilin University, Changchun 130012, China. E-mail: yanw@jlu.edu.cn
[b]Chongqing Key Laboratory of Green Catalytic Materials and Technology, College of Chemistry, Chongqing Normal University, Chongqing 401331, China
[c]SINOPEC (Dalian) Research Institute of Petroleum and Petrochemicals Co., Ltd, Dalian 116045, P.R China. E-mail: liuchang.fshy@sinopec.com

Open Access Article. Published on 19 January 2026. Downloaded on 2/25/2026 1:52:34 AM. This article is licensed under a Creative Commons Attribution-NonCommercial 3.0 Unported Licence.

Therefore, methanol amination is governed by three key parameters: acid concentration, acid strength, and acid site distribution. These can be tuned by adjusting the Si/Al ratio and the distribution of framework Al.[5,14] Among 8MR zeolites, the **CHA** framework is especially promising. Its small pores hinder the formation and diffusion of bulky by-products and coke precursors, enabling high selectivity and long catalytic lifetimes.[15,16] For example, SAPO-34 and SSZ-13—both **CHA**-type zeolites—exhibit excellent light olefin selectivity and stability in methanol-to-olefins (MTO) reactions.[17–19] These structural advantages suggest that **CHA** could be optimized for methanol amination by precisely controlling its Si/Al ratio and Al distribution.

Several strategies have been explored to tune Si/Al ratios and Al distributions in **CHA**, including variation of alkali cations,[20] gel composition,[21–23] seed crystals,[24] and OSDAs.[25] OSDA-free synthesis is both more economical and environmentally sustainable. However, under OSDA-free conditions, achieving precise control and Si/Al ratios and Al distributions—and understanding their catalytic impact—remain challenging.[24,26]

Another persistent challenge is the unavoidable formation of DME as a major by-product. Separating and recovering DME increases process complexity and cost.[27] Although adjusting operating parameters such as the ammonia-to-methanol ratio (N/C) and space velocity can partially suppress DME formation, eliminating it through catalyst design remains an open challenge.[7,11]

In this study, we developed a strategy to regulate Si/Al ratios and Al distributions in **CHA** zeolites under OSDA-free conditions. The synthesis combined alkali cations with seed crystals of varying Al contents (SAPO-34, SSZ-13, and pure silica **CHA**). Cesium cations promoted **CHA** crystallization across a broad Si/Al range. The Al content and dosage of the seed controlled the Si/Al ratio of the final product, while the seed type determined the Al distribution.

Catalytic testing revealed that at the same Si/Al ratio (3.8), the sample synthesized with SAPO-34 seed (CHA-S34-3.8) achieved higher MMA and DMA selectivity than the sample synthesized with pure silica **CHA** seed (CHA-PS-3.8). Remarkably, no DME was detected under steady-state conditions. Characterization confirmed that CHA-S34-3.8 had a higher fraction of Al located in the 8MRs, as evidenced by Co^{2+} titration and UV–vis spectroscopy. NH_3-TPD showed a high density of acid sites with moderate strength, explaining its superior performance.

Overall, this work demonstrates that tailoring Al distribution through seed selection provides an effective strategy to enhance methanol amination. By combining optimal Si/Al ratios with targeted Al placement in the **CHA** framework, high MMA and DMA selectivity can be achieved while completely suppressing DME formation.

2. Results and discussion

2.1 Synthesis and characterization of CHA seeds

SAPO-34, SSZ-13 and pure silica **CHA** (PS-CHA) seeds with different Al contents were synthesized (Fig. S1; synthesis in SI). Powder X-ray diffraction (XRD, Fig. S1a and b) confirmed that all seeds were pure **CHA**, both before and after calcination, yielding c-SAPO-34, c-SSZ-13, and c-PS-CHA. Thermogravimetric (TG) analysis (Fig. S1c) showed weight loss below 200 °C from physiosorbed water and between 200–800 °C from OSDA decomposition. Combined ICP-OES and TG analyses gave Al_2O_3 contents of 30.4% (SAPO-34), 9.4% (SSZ-13), and 0% (PS-CHA). Scanning electron microscope (SEM) images (Fig. S1d–f) revealed cubic morphologies with sizes of ~15 μm (SAPO-34), ~240 nm (SSZ-13), and ~20 μm (PS-CHA).

2.2 Synthesis and characterizations of CHA zeolites

Five **CHA** zeolites were synthesized OSDA-free using a gel of 20 SiO_2 : 1 Al_2O_3 : 6 Na_2O : 1 Cs_2O : 2000 H_2O and 20 wt.% seed. Products were named CHA-S34-3.4, CHA-S13-4.1, and CHA-PS-4.3, where the final number denotes the Si/Al ratio. By tuning gel composition, CHA-S34-3.8 and CHA-PS-3.8 were also obtained.

XRD confirmed high crystallinity in all samples (Fig. 1a). SEM showed aggregates of irregular grains (Fig. S2). N_2 adsorption isotherms (Fig. 1b) were type I, with micropore areas of 713–745 m^2 g^{-1} and volumes of 0.257–0.265 cm^3 g^{-1} (Table 1), consistent with literature.[28] ^{29}Si MAS NMR (Fig. 1c) showed signals at −99, −105, and −110 ppm, corresponding to Si (2Si, 2Al), Si (3Si, 1Al), and Si (4Si, 0Al), respectively.[29] Gaussian deconvolution yielded Si species distributions and Si/Al rations (Table S1), which matched ICP-OES results (Table 1). ^{27}Al MAS NMR (Fig. 1d) exhibited only tetrahedral Al at 59 ppm. For CHA-S34-3.4 and CHA-S34-3.8, ^{31}P MAS NMR (Fig. S3) and ICP-OES confirmed no phosphorus incorporation from SAPO-34 seeds.

Elemental analysis detected little C or N in SAPO-34- or SSZ-13-derived **CHA**. In contrast, CHA-PS-4.3 and CHA-PS-3.8 contained 3.51 and 2.9 wt.% C, respectively, indicating OSDA

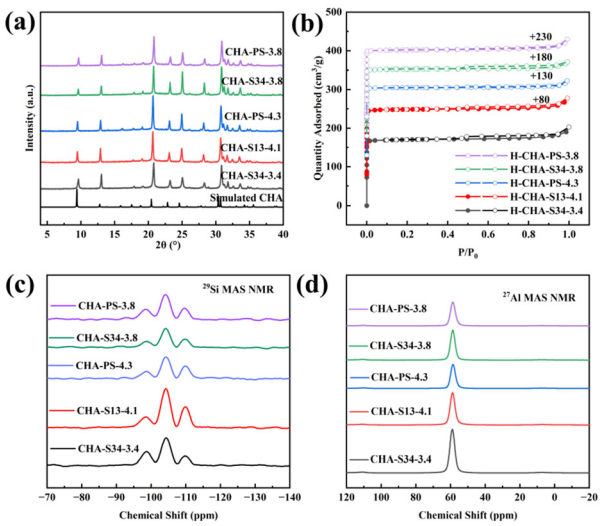

Fig. 1 (a) Experimental and simulated XRD patterns of the **CHA** zeolites, (b) N_2 adsorption–desorption isotherms of the H form the **CHA** zeolites at 77 K, (c) ^{29}Si MAS NMR spectra of the as-synthesized **CHA** zeolites, (d) ^{27}Al MAS NMR spectra of the as-synthesized **CHA** zeolites.

This journal is © the Partner Organisations 2026

Open Access Article. Published on 19 January 2026. Downloaded on 2/25/2026 1:52:34 AM.
This article is licensed under a Creative Commons Attribution-NonCommercial 3.0 Unported Licence.

Table 1 Si/Al ratios and BET surface areas of the **CHA** zeolites

Sample	Si/Al[a]	Si/Al[b]	S_{BET} [c] ($m^2\ g^{-1}$)	S_{micro} ($m^2\ g^{-1}$)	V_{total} ($cm^3\ g^{-1}$)	V_{micro} [d] ($cm^3\ g^{-1}$)
CHA-S34-3.4	3.4	3.5	716	703	0.301	0.258
CHA-S13-4.1	4.1	4.3	713	703	0.305	0.257
CHA-PS-4.3	4.3	4.3	745	731	0.298	0.265
CHA-S34-3.8	3.8	4.0	731	722	0.294	0.263
CHA-PS-3.8	3.8	3.8	731	722	0.308	0.263

[a] Determined by the ICP-OES analyses. [b] Determined by the ^{29}Si NMR MAS analyses. [c] All samples are H-type. [d] T-plot method.

incorporation from PS-CHA seeds. TG profiles (Fig. S4) supported this conclusion. PS-CHA-seeded samples showed two weight-loss steps, including one above 400 °C from OSDA removal, while SAPO-34- and SSZ-13-derived samples displayed only dehydration.[30]

2.3 Crystallization process

To probe crystallization, we examined CHA-S34-3.4, CHA-S13-4.1, and CHA-PS-4.3, synthesized from identical gels but different seeds. At 0 h, XRD (Fig. 2a, c and e) showed that SSZ-13 and PS-CHA seeds retained **CHA** diffraction, whereas SAPO-34 appeared amorphous. By 9 h, all systems began crystallizing, and by 18 h, full **CHA** crystallinity was achieved. A transient **GIS** phase was observed in PS-CHA (3–12 h) but later disappeared. Crystallization curves showed sigmoidal growth kinetics (Fig. 2b, d and f).[31]

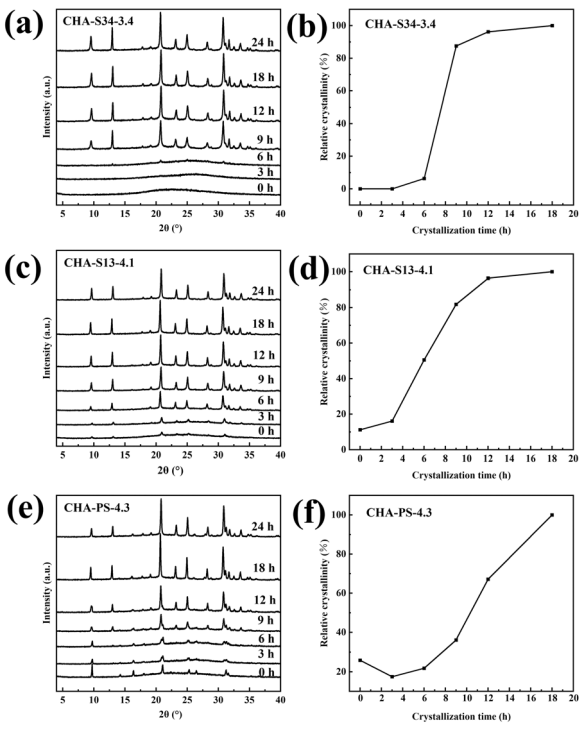

Fig. 2 XRD patterns of the solid products with the varied crystallization time of (a) CHA-S34-3.4, (c) CHA-S13-4.1, and (e) CHA-PS-4.3 and the corresponding curves of (b) CHA-S34-3.4, (d) CHA-S13-4.1, and (f) CHA-PS-4.3.

SEM (Fig. S5–S7) revealed a non-classical crystallization pathway: seed dissolution at 0 h, nanoparticle formation by 3–6 h, aggregation by 6–12 h, and assembly into nanograins by 18 h.[32] Notably, the grain size of the crystallized products decreases systematically with increasing Al content in the seed. This trend is attributed to the higher solubility of SAPO-34 in alkaline media, which generates a large number of nucleation sites during the early stage of crystallization.

FT-IR spectroscopy tracked short-range structural evolution (Fig. 3a–c). Bands near 780 and 720 cm^{-1} corresponded to Si–O–Si and Si–O–Al vibrations in single 4-membered rings (*s4r*). Bands at ~650 and ~540 cm^{-1} were assigned to double 6-membered rings (*d6r*).[33] After 3 h, s4r signals appeared, indicating amorphous aluminosilicate nuclei with short-range order. Characteristic d6r signals of **CHA**, appeared earlier with SSZ-13 and PS-CHA seeds (3 h) but only after 9 h with SAPO-34, consistent with its slower crystallization in XRD.[34]

2.4 Influence of synthesis parameters

2.4.1 Role of alkali cations. Without seeds, Na^+ and K^+ gels gave only amorphous products. With seeds, Na^+ produced **PHI** (SAPO-34), **CHA** + **MOR** (SSZ-13), and **CHA** + **GIS** (PS-CHA). K^+ yielded pure **CHA** with SAPO-34 and SSZ-13 (Si/Al = 3.0 and 3.2, respectively), but **CHA** + **ERI** with PS-CHA. Strikingly, Cs^+

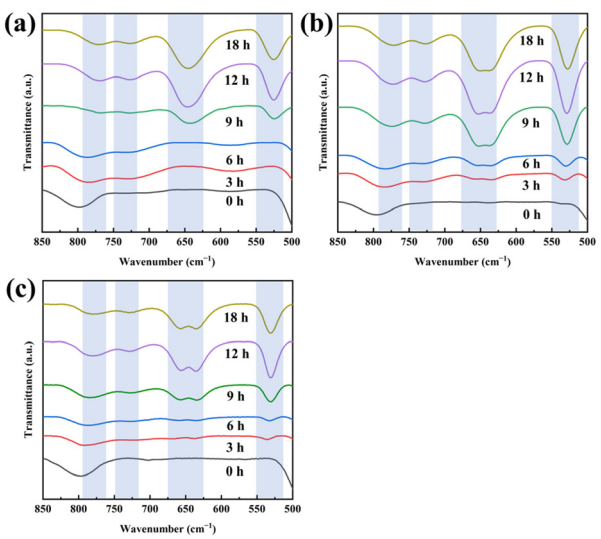

Fig. 3 FT-IR spectra of the isolated solid samples throughout the crystallization of (a) CHA-S34-3.4, (b) CHA-S13-4.1, and (c) CHA-PS-4.3.

Open Access Article. Published on 19 January 2026. Downloaded on 2/25/2026 1:52:34 AM. This article is licensed under a Creative Commons Attribution-NonCommercial 3.0 Unported Licence.

enabled pure **CHA** crystallization even without seeds, attributed to its larger radius and lower charge density.[35] With Cs^+ and seeds, **CHA** formed with Si/Al ratios of 3.4 (SAPO-34), 4.1 (SSZ-13), and 4.3 (PS-CHA) (Fig. 4a–c).

2.4.2 Role of seed dosage. In Na–Cs systems, seed dosage (5–20%) directly controlled Si/Al ratios (Fig. 4d–f and Table S2).

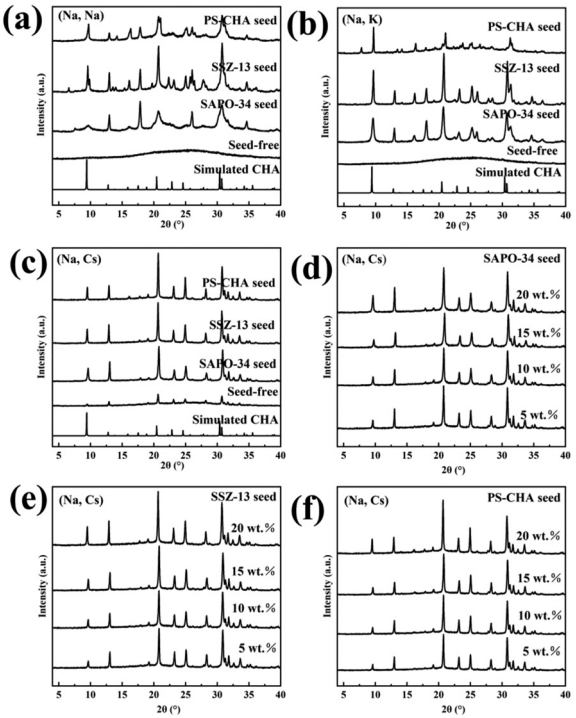

Fig. 4 XRD patterns of products from the (a) Na–Na, (b) Na–K, and (c) Na–Cs systems, with and without seed crystals. XRD patterns of the products obtained by adding different contents of (d) SAPO-34 seed crystals, (e) SSZ-13 seed crystals, and (f) PS-CHA seed crystals.

SAPO-34 seeds lowered the Si/Al ratio with increasing dosage, whereas SSZ-13 and PS-CHA seeds increased it. At 5% dosage, Si/Al was ~3.6–3.7; at 20%, values reached 3.4 (SAPO-34), 4.1 (SSZ-13), and 4.3 (PS-CHA). Seeds thus acted as both nucleation inducers and Si/Al sources, enabling systematic composition control. Three 20%-seeded products were selected for catalysis.

2.4.3 Role of OSDAs. We next examined the influence of OSDAs retained in the seeds. Calcined SAPO-34 (c-SAPO-34) and SSZ-13 (c-SSZ-13) still yielded pure **CHA** with unchanged morphology (Fig. S8a and S9a, b), showing that their OSDAs did not contribute to crystallization. In contrast, calcined PS-CHA (c-PS-CHA) produced only amorphous material, confirming that its OSDA was essential. When seeds were replaced by equivalent raw materials plus OSDAs, pure **CHA** formed only in PS-CHA-derived mixtures (Fig. S8c and d). SEM revealed morphology changes depending on crystallization pathway (Fig. S9c and d).

Why do c-SAPO-34 and c-SSZ-13 still yield **CHA**, while c-PS-CHA fails? XRD at 0 h (Fig. S8b) showed that c-SAPO-34 and c-SSZ-13 resembled their uncalcined counterparts, retaining amorphous and **CHA** features. In contrast, c-PS-CHA-derived gels were fully amorphous. As shown in Fig. 2c, uncalcined PS-CHA displayed **CHA** peaks at 0 h, whereas c-PS-CHA did not, suggesting seed dissolution after calcination.

Previous studies indicate that negatively charged AlO_4^- units and OSDAs stabilize frameworks against OH^- attack, preserving locally ordered species that promote crystallization.[36–38] After calcination, c-SAPO-34 and c-SSZ-13 retain AlO_4^-, while c-PS-CHA lacks both AlO_4^- and OSDAs. Consequently, c-PS-CHA cannot maintain sufficient short-range order to initiate **CHA** crystallization. These results highlight the dual role of OSDA in PS-CHA: directing framework formation and protecting seeds from dissolution, thereby preserving precursor species essential for **CHA** crystallization.

Table 2 Comparison of catalytic performance of **CHA** zeolites for selective synthesis of methylamine under two conditions

Sample	N/C[a]	$WHSV_{MeOH}$[b] (h^{-1})	T (°C)	MeOH conversion (%)	Selectivity (%)					(MMA + DMA) Yield[c] (%)
					MMA	DMA	MMA + DMA	TMA	DME	
H-CHA-S34-3.4	2	0.813	350	99.6	38.8	40.3	79.1	17.5	2.0	78.8
H-CHA-S13-4.1	2	0.813	350	99.4	31.9	54.3	86.2	7.9	5.0	85.7
H-CHA-PS-4.3	2	0.813	350	97.6	30.5	54.7	85.2	8.9	5.1	83.2
H-CHA-S34-3.8	2	0.813	350	98.8	33.3	54.4	87.7	11.6	0	86.6
H-CHA-PS-3.8	2	0.813	350	97.7	29.0	53.7	82.7	11.5	5.1	80.8
H-CHA-S34-3.4	1	4.3	400	98.6	21.5	55.5	77.0	17.8	4.2	75.9
H-CHA-S13-4.1	1	4.3	400	98.9	26.5	57.9	84.4	8.6	5.8	83.5
H-CHA-PS-4.3	1	4.3	400	98.6	25.9	60.4	86.3	7.4	4.3	84.8
H-CHA-S34-3.8	1	4.3	400	98.8	24.8	63.9	88.7	10.5	0	87.6
H-CHA-PS-3.8	1	4.3	400	98.9	25.3	55.8	81.1	13.6	4.2	80.2

[a] Molar ratio of the feed gas composition. [b] Time on stream = 7 h. [c] MMA plus DMA yield = MeOH conversion × MMA plus DMA selectivity in all carbon base products.

This journal is © the Partner Organisations 2026

Open Access Article. Published on 19 January 2026. Downloaded on 2/25/2026 1:52:34 AM.
This article is licensed under a Creative Commons Attribution-NonCommercial 3.0 Unported Licence.

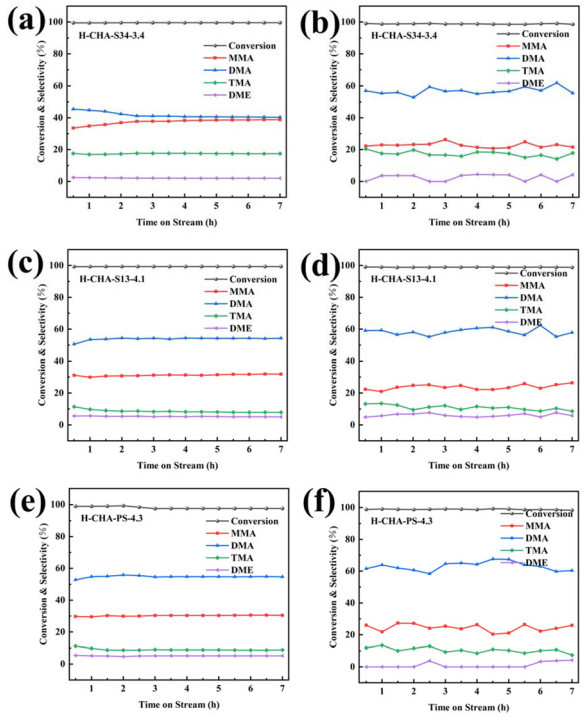

Fig. 5 Methanol amination over (a, c and e) H-CHA-S34-3.4, H-CHA-S13-4.1, and H-CHA-PS-4.3 at 350 °C, N/C = 2, $WHSV_{MeOH}$ = 0.813 h^{-1}; and (b, d and f) the same catalysts at 400 °C, N/C = 1, $WHSV_{MeOH}$ = 4.3 h^{-1}. Plots show methanol conversion and product selectivity.

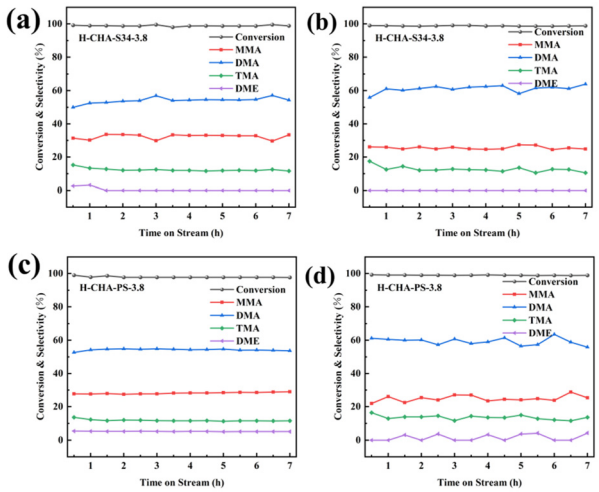

Fig. 6 Methanol amination over (a and c) H-CHA-S34-3.8, and H-CHA-PS-3.8 at 350 °C, N/C = 2, $WHSV_{MeOH}$ = 0.813 h^{-1}; and (b and d) the same catalysts at 400 °C, N/C = 1, $WHSV_{MeOH}$ = 4.3 h^{-1}. Plots show methanol conversion and product selectivity.

2.5 Catalytic performance of CHA zeolites

The catalytic activity of five **CHA** zeolites—H-CHA-S34-3.4, H-CHA-S13-4.1, H-CHA-PS-4.3, H-CHA-S34-3.8, and H-CHA-PS-3.8—was tested under two conditions: (i) 350 °C, N/C = 2, $WHSV_{MeOH}$ = 0.813 h^{-1} and (ii) 400 °C, N/C = 1, $WHSV_{MeOH}$ = 4.3 h^{-1}. Results are summarized in Table 2, with product trends shown in Fig. 5 and 6.

At 350 °C, all catalysts showed stable product distributions, whereas at 400 °C, fluctuation were more pronounced. In both cases, methanol conversion exceeded 97%. The main differences appeared in product selectivity.

For H-CHA-S34-3.4, H-CHA-S13-4.1, and H-CHA-PS-4.3, increasing the Si/Al ratio (3.4 → 4.3) enhanced MMA + DMA selectivity, lowered TMA selectivity, but increased DME formation. Thus, a higher Si/Al ratio suppressed TMA but promoted DME. Notably, H-CHA-S34-3.8 deviated from this trend: despite having a higher Si/Al ratio than H-CHA-S34-3.4, it showed reduced TMA selectivity and no detectable DME. By

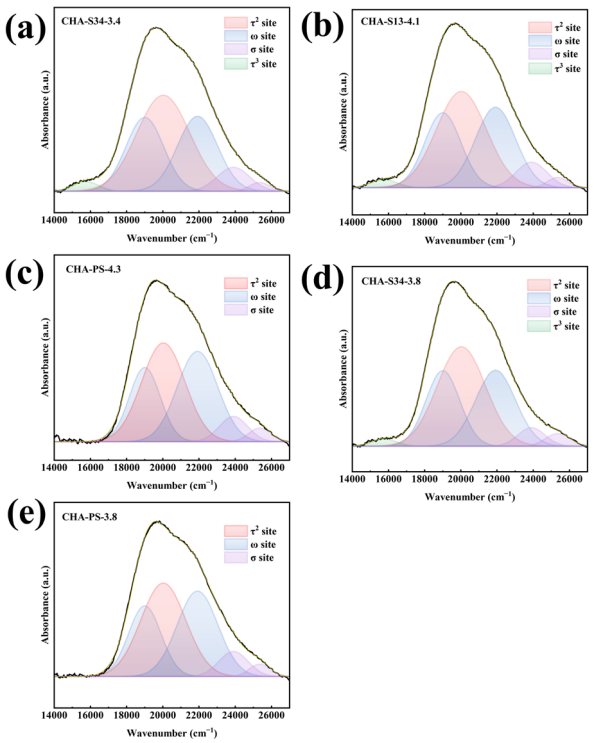

Fig. 7 UV–vis spectra of Co^{2+} exchanged (a) CHA-S34-3.4, (b) CHA-S13-4.1, (c) CHA-PS-4.3, (d) CHA-S34-3.8, and (e) CHA-PS-3.8.

Table 3 Al distribution in **CHA** zeolites

Sample	Co/Al[a]	Isolated Al (%)	Paired Al (%)			
			Total	τ^{2Si}	ω	σ
Co-CHA-S34-3.4	0.38	24	76	33.5	36.5	6.0
Co-CHA-S13-4.1	0.38	24	76	31.9	37.8	6.3
Co-CHA-PS-4.3	0.38	24	76	28.9	40.3	6.8
Co-CHA-S34-3.8	0.38	24	76	33.2	37.4	5.4
Co-CHA-PS-3.8	0.38	24	76	29.1	40.1	6.8

[a] Determined by the ICP-OES analyses.

Open Access Article. Published on 19 January 2026. Downloaded on 2/25/2026 1:52:34 AM. This article is licensed under a Creative Commons Attribution-NonCommercial 3.0 Unported Licence.

Table 4 Comparison of catalytic performances of zeolitic catalysts on selective synthesis of methylamine under various conditions

Sample	Time on stream (h)	N/C	$WHSV_{MeOH}$ (h^{-1})	T (°C)	MeOH conversion (%)	Selectivity (%)			(MMA + DMA) Yield (%)	Ref.
						MMA	DMA	TMA		
H-CHA-S34-3.8	**7**	**2**	**0.813**	**350**	**98.8**	**33.3**	**54.4**	**11.6**	**86.6**	**This work**
H-CHA-S34-3.8	**7**	**1**	**4.3**	**400**	**98.8**	**24.8**	**63.9**	**10.5**	**87.6**	**This work**
H-RHO-8.7	3	2	0.813	350	96.8	—	—	13.59	75.3	11
H-RHO-7.3	3	2	0.813	350	98.1	—	—	12.99	74.1	11
H-RHO-8.7	10	1	4.3	400	95.9	—	—	11.05	65.4	11
H-RHO-7.3	10	1	4.3	400	96.9	—	—	13.31	69.4	11
H-ZK-5	3	2	0.813	350	63.4	33.7	52.5	5.1	54.7	13
D-20	12	2	0.813	320	91.4	22.3	60.9	11.3	76.0	19
D-20–700 °C	12	2	0.813	320	82.2	25.0	64.3	5.2	73.4	19
D-20–800 °C	12	2	0.813	320	65.2	29.6	55.7	4.1	55.6	19
H-DNL-6	2.4	2	0.813	300	88.3	26.1	45.9	12.5	63.6	41
M-DNL-6	2.4	2	0.813	300	80.0	24.4	50.7	17.5	60.1	41
L-DNL-6	2.4	2	0.813	300	82.9	21.3	31.9	36.1	44.1	41
SAPO-34	2.8	2	0.813	380	82.0	26.8	54.7	14.5	66.8	9

contrast, H-CHA-PS-3.8 (same Si/Al = 3.8) produced significant DME, indicating that Al distribution—determined by seed—was as important as the Si/Al ratio.

2.5.1 Correlation with acid properties. Acidity is a key factor in methanol amination.[8] NH_3-TPD profiles (Fig. S10) were deconvoluted into weak, medium, and strong sites (Table S3).[39] High acid density promoted deeper methylation, giving higher TMA selectivity. At the same time, abundant acid sites generated more alkylammonium ions, which occupied pore volume and suppressed DME formation.[9,27] For example, H-CHA-S34-3.4 had the highest acid density, consistent with its high TMA selectivity and low DME yield.

Previous studies suggested that reducing acid density decreases alkylammonium ion formation, leaving more void space for TMA production and diffusion. Strong acidity, on the other hand, drives continuous methylation to TMA.[3] In our case, this effect was less evident, likely because the investigated Si/Al ratios covered only a narrow range.[7]

2.5.2 Influence of aluminium distribution. Brønsted acidity originates from framework Al, and its distribution strongly affects catalysis. To probe Al siting, Co^{2+} exchange—a standard method to quantify Al pairing—was performed. The amount of Co^{2+} exchanged reflects the population of Al pairs at specific crystallographic sites. In **CHA**, Al pairs can occupy τ (τ^{2Si}, τ^{3Si}) sites in 8MRs, ω sites in d6r unit, and σ sites in 6MRs.[24,25,40]

UV–vis spectra of Co^{2+}-exchanged samples (Fig. 7), deconvoluted by Gaussian fitting, revealed systematic variations in Al distributions (Table 3). While the total fraction of paired Al sites was comparable across all samples, their spatial distribution depended strongly on the seed. The similar paired Al contents likely reflect thermodynamic stabilization dominated by alkali metal cations. SAPO-34-derived **CHA** (CHA-S34-3.4, CHA-S34-3.8) showed higher τ^{2Si} fractions and lower ω fractions, indicating preferential Al placement in 8MRs. In contrast, PS-CHA-derived **CHA** (CHA-PS-4.3, CHA-PS-3.8) displayed the opposite trend. SSZ-13-derived **CHA** (CHA-S13-4.1) exhibited intermediate behavior. These differences arise from the greater abundance aluminosilicate species generated by SAPO-34 during the early stage of crystallization. This enhanced availability provides a kinetic advantage for the incorporation of paired Al into the **CHA** framework. SSZ-13 and PS-CHA seeds follow the same trend with progressively weaker effects.

This distinction was clearest between H-CHA-S34-3.8 and H-CHA-PS-3.8 (Si/Al = 3.8). The former contained more τ^{2Si} Al pairs, enriching Brønsted acid sites in 8MRs. This distribution explains its unique performance: suppressed TMA selectivity and complete elimination of DME.

2.5.3 Benchmarking against reported catalysts. The performance of H-CHA-S34-3.8 was compared with reported methanol amination catalysts under similar conditions (Table 4). Although all systems achieved high conversion, H-CHA-S34-3.8 delivered superior MMA + DMA yield and, importantly, no DME. These results highlight the decisive role of Al distribution—particularly enrichment in 8MRs—in dictating selectivity.

3. Conclusion

CHA zeolites were synthesized without OSDAs by combining alkali cations with seeds of varying Al contents. Cs^+, owing to its low charge density, promoted **CHA** crystallization across a wide Si/Al ratio range. Seed type and dosage allowed precise control over Si/Al ratio and Al distribution.

Catalytic testing demonstrated that both acidity and Al distribution govern methanol amination. Among all samples, H-CHA-S34-3.8 was the most effective, combining high MMA + DMA yield with negligible DME formation. This performance was linked to its high acid density, moderate acid strength, and preferential Al placement in 8MRs.

In summary, this study presents a simple and effective route to tailor Al content and distribution in **CHA** zeolites,

 This journal is © the Partner Organisations 2026

Open Access Article. Published on 19 January 2026. Downloaded on 2/25/2026 1:52:34 AM. This article is licensed under a Creative Commons Attribution-NonCommercial 3.0 Unported Licence.

offering a promising design strategy for high-performance methanol amination catalysts.

Author contributions

Shuang Liu: writing – original draft, formal analysis, data curation. Pan Xu: validation, data curation. Sihui Li: software, methodology. Junyao Pan: visualization, formal analysis, data curation. Yuxin Yan: investigation, formal analysis. Rui Wu: formal analysis, data curation. Junhui Guo: investigation, formal analysis. Chang Liu: writing – review & editing, supervision. Wenfu Yan: writing – review & editing, supervision, funding acquisition, conceptualization.

Conflicts of interest

There are no conflicts to declare.

Data availability

The data supporting this article have been included as part of the supplementary information (SI). Supplementary information is available. Supplementary information: materials, synthesis, characterization, ion exchange process, catalytic tests, and additional data. See DOI: **https://doi.org/10.1039/d5qi02464a**.

Acknowledgements

We acknowledge the financial support from the National Key Research and Development Program of China (2024YFE0201000), the National Natural Science Foundation of China (22288101), the '111 Center' (B17020) and the Technology Development Contract of Sinopec (Grant No. 123092) for supporting this work.

References

1 D. R. Corbin, S. Schwarz and G. C. Sonnichsen, Methylamines synthesis: A review, *Catal. Today*, 1997, **37**, 71–102.
2 K. S. Hayes, Industrial processes for manufacturing amines, *Appl. Catal., A*, 2001, **221**, 187–195.
3 I. Mochida, A. Yasutake, H. Fujitsu and K. Takeshita, Selective synthesis of dimethylamine (DMA) from methanol and ammonia over zeolites, *J. Catal.*, 1983, **82**, 313–321.
4 K. Y. Jin, Y. Yan, J. Pan, J.-Y. Liu and W. Yan, The Application of Zeolites in the Selective Synthesis of Methylamine: A Review, *Catalysts*, 2025, **15**, 294.
5 J. Li, M. Gao, W. Yan and J. Yu, Regulation of the Si/Al ratios and Al distributions of zeolites and their impact on properties, *Chem. Sci.*, 2023, **14**, 1935–1959.
6 B. Y. Wang, Y. Yan, X. Zhou, H. Su, H. Zhang, J.-N. Zhang, J. Xu, Q. Pan and W. Yan, Mild activation of spent fluid catalytic cracking (FCC) catalysts for the pilot synthesis of zeolite a with commercial quality and excellent Co^{2+} removal, *Chem. Eng. J.*, 2024, **490**, 151733.
7 Y. Sasaki and M. Fukatsu, Selective catalysts for the production of nitrogen-containing compounds, *Catal. Surv. Jpn.*, 1998, **2**, 199–205.
8 H. Y. Jeon, C. H. Shin, H. J. Jung and S. B. Hong, Catalytic evaluation of small-pore molecular sieves with different framework topologies for the synthesis of methylamines, *Appl. Catal., A*, 2006, **305**, 70–78.
9 Y. Qiao, P. Wu, X. Xiang, M. Yang, Q. Wang, P. Tian and Z. Liu, SAPO-34 synthesized with n-butylamine as a template and its catalytic application in the methanol amination reaction, *Chin. J. Catal.*, 2017, **38**, 574–582.
10 H. Lee, K. Lee, J. Shin and S. B. Hong, A comparative study of methylamines synthesis over zeolites H-rho and H-PST-29, *Microporous Mesoporous Mater.*, 2020, **300**, 110150.
11 Y. Wang, J. Han, K. Jin, S. Liu, Q. Li, P. Hou, S. Liu, Q. Song, Z. Wang, P. Tian and W. Yan, Fluoride-free synthesis of high-silica RHO zeolite for the highly selective synthesis of methylamine, *Inorg. Chem. Front.*, 2024, **11**, 5473–5483.
12 S. H. Ahn, D. Shu and S. B. Hong, Synthesis of stable ECR-18 zeolite and its catalytic properties in methanol amination, *Microporous Mesoporous Mater.*, 2024, **364**, 112875.
13 R. Wu, J. Han, Y. Wang, M. Chen, P. Tian, X. Zhou, J. Xu, J.-N. Zhang and W. Yan, Exclusive SAPO-seeded synthesis of ZK-5 zeolite for selective synthesis of methylamines, *Inorg. Chem. Front.*, 2022, **9**, 5766–5773.
14 P. Xiao, L. Wang, H. Toyoda, Y. Wang, K. Nakamura, J. Huang, R. Osuga, M. Nishibori, H. Gies and T. Yokoi, Revealing Active Sites and Reaction Pathways in Direct Oxidation of Methane over Fe-Containing CHA Zeolites Affected by the Al Arrangement, *J. Am. Chem. Soc.*, 2024, **146**, 31969–31981.
15 M. Dusselier and M. E. Davis, Small-Pore Zeolites: Synthesis and Catalysis, *Chem. Rev.*, 2018, **118**, 5265–5329.
16 M. Sarker, N. A. Khan, D. K. Yoo, B. N. Bhadra, J. W. Jun, T. W. Kim, C. U. Kim and S. H. Jhung, Synthesis of SSZ-13 zeolite in the presence of dimethylethylcyclohexyl ammonium ion and direct conversion of ethylene to propylene with the SSZ-13, *Chem. Eng. J.*, 2019, **377**, 120116.
17 F. Bleken, M. Bjorgen, L. Palumbo, S. Bordiga, S. Svelle, K.-P. Lillerud and U. Olsbye, The Effect of Acid Strength on the Conversion of Methanol to Olefins Over Acidic Microporous Catalysts with the CHA Topology, *Top. Catal.*, 2009, **52**, 218–228.
18 X. Zhu, Y. Gao, H. Chen, M. Jiang, X. Wang, C. Miao, Y. Shen, Y. Ji, Z. Qin, Z. Wu, W. Song, C. Xu and B. Shen, Constructing Hierarchical Zeolites with Highly Complete Framework via Controlled Desilication, *Angew. Chem., Int. Ed.*, 2024, **63**, e202411446.

Open Access Article. Published on 19 January 2026. Downloaded on 2/25/2026 1:52:34 AM. This article is licensed under a Creative Commons Attribution-NonCommercial 3.0 Unported Licence.

19 Z. Liu, Q. Wang, S. Liu, M. Yang, D. Fan, D. Zhu and P. Tian, Synthesis of SAPO-34 by utilizing spent industrial MTO catalyst and their catalytic applications, *Mater. Today Sustain.*, 2023, **21**, 100302.
20 W. Lv, S. Wang, P. Wang, Y. Liu, Z. Huang, J. Li, M. Dong, J. Wang and W. Fan, Regulation of Al distributions and Cu^{2+} locations in SSZ-13 zeolites for NH_3-SCR of NO by different alkali metal cations, *J. Catal.*, 2021, **393**, 190–201.
21 T. Nishitoba, N. Yoshida, J. N. Kondo and T. Yokoi, Control of Al Distribution in the CHA-Type Aluminosilicate Zeolites and Its Impact on the Hydrothermal Stability and Catalytic Properties, *Ind. Eng. Chem. Res.*, 2018, **57**, 3914–3922.
22 W. Lv, P. Meng, Z. Qin, J. Li, M. Dong, J. Wang and W. Fan, A comparison of Al-rich Cu-SSZ-13 zeolites synthesized by different methods in their Al distribution, hydrothermal stability and catalytic performance in the selective catalytic reduction of NO_x with NH_3, *Microporous Mesoporous Mater.*, 2021, **313**, 110851.
23 K. Nakamura, P. Xiao, R. Osuga, Y. Wang, S. Yasuda, T. Matsumoto, J. N. Kondo, M. Yabushita, A. Muramatsu, H. Gies and T. Yokoi, Impacts of framework Al distribution and acidic properties of Cu-exchanged CHA-type zeolite on catalytic conversion of methane into methanol followed by lower hydrocarbons, *Catal. Sci. Technol.*, 2023, **13**, 2648–2651.
24 Y. Wang, J. Han, M. Chen, W. Lv, P. Meng, W. Gao, X. Meng, W. Fan, J. Xu, W. Yan and J. Yu, Low-silica Cu-CHA Zeolite Enriched with Al Pairs Transcribed from Silicoaluminophosphate Seed: Synthesis and Ammonia Selective Catalytic Reduction Performance, *Angew. Chem., Int. Ed.*, 2023, **62**, e20230617.
25 J. Zhang, Y. Shan, L. Zhang, J. Du, H. He, S. Han, C. Lei, S. Wang, W. Fan, Z. Feng, X. Liu, X. Meng and F.-S. Xiao, Importance of controllable Al sites in CHA framework by crystallization pathways for NH3-SCR reaction, *Appl. Catal., B*, 2020, **277**, 119193.
26 H. Imai, N. Hayashida, T. Yokoi and T. Tatsumi, Direct crystallization of CHA-type zeolite from amorphous aluminosilicate gel by seed-assisted method in the absence of organic-structure-directing agents, *Microporous Mesoporous Mater.*, 2014, **196**, 341–348.
27 V. A. Veefkind, C. Grundling and J. A. Lercher, Steric aspects in methylamine and dimethylether synthesis over acidic mordenites, *J. Mol. Catal. A:Chem.*, 1998, **134**, 111–119.
28 W. Wang, W. Li, Z. Wang, B. Liu, B. Wang, J. Duan and R. Zhou, Directly synthesized high-silica CHA zeolite for efficient CO_2/N_2 separation, *J. Environ. Chem. Eng.*, 2024, **12**, 113036.
29 M. Debost, P. B. Klar, N. Barrier, E. B. Clatworthy, J. Grand, F. Laine, P. Brazda, L. Palatinus, N. Nesterenko, P. Boullay and S. Mintova, Synthesis of Discrete CHA Zeolite Nanocrystals without Organic Templates for Selective CO_2 Capture, *Angew. Chem., Int. Ed.*, 2020, **59**, 23491–23495.
30 L. Bing, A. Tian, F. Wang, K. Yi, X. Sun and G. Wang, Template-Free Synthesis of Hierarchical SSZ-13 Microspheres with High MTO Catalytic Activity, *Chem. – Eur. J.*, 2018, **24**, 7428–7433.
31 K. Du, X. Zhang, T. He, W. Shen, H. Xu, Y. Tang, X.-M. Cao, Z. Huang and Y. Zhang, Dynamic Evolution of Structural Ordering and Aluminum Redistribution During ZSM-5 Zeolite Crystallization, *Angew. Chem., Int. Ed.*, 2025, **64**, e202507223.
32 H. Li, J. Yu, K. Du, W. Li, L. Ding, W. Chen, S. Xie, Y. Zhang and Y. Tang, Synthesis of ZSM-5 Zeolite Nanosheets with Tunable Silanol Nest Contents across an Ultra-wide pH Range and Their Catalytic Validation, *Angew. Chem., Int. Ed.*, 2024, **63**, e202405092.
33 Z. Zhang, Y. Li, Z. Chen, F. Ji, X. Liang, H. Xuan, L. Han and P. Han, TEAOH-assisted cost-effective preparation of SSZ-13 using L zeolite as Al source, *Fuel*, 2024, **362**, 130885.
34 S. Ghojavand, E. B. Clatworthy, A. Vicente, E. Dib, V. Ruaux, M. Debost, J. El Fallah and S. Mintova, The role of mixed alkali metal cations on the formation of nano-sized CHA zeolite from colloidal precursor suspension, *J. Colloid Interface Sci.*, 2021, **604**, 350–357.
35 Z. Mi, S. Li, W. Liu, J. Wang, D. Deng, P. Liu, P. Tian, C. Liu, W. Yan, K. Zhu, Z. Wang, Z. Liu and J. Yu, Direct Synthesis of Highly Siliceous Faujasite-type Zeolite Enabled by Low Charge Density Organic Structure-directing Agents, *J. Am. Chem. Soc.*, 2025, **147**, 16922–16934.
36 K. Honda, A. Yashiki, M. Itakura, Y. Ide, M. Sadakane and T. Sano, Influence of seeding on FAU-*BEA interzeolite conversions, *Microporous Mesoporous Mater.*, 2011, **142**, 161–167.
37 J. C. Groen, J. C. Jansen, J. A. Moulijn and J. Pérez-Ramírez, Optimal aluminum-assisted mesoporosity development in MFI zeolites by desilication, *J. Phys. Chem. B*, 2004, **108**, 13062–13065.
38 H. Zhang, B. Wang and W. Yan, The structure-directing role of heterologous seeds in the synthesis of zeolite, *Green Energy Environ.*, 2024, **9**, 792–801.
39 J. Han, J. Li, W. Zhao, L. Li, M. Chen, X. Ge, S. Wang, Q. Liu, D. Mei and J. Yu, Cu-OFF/ERI Zeolite: Intergrowth Structure Synergistically Boosting Selective Catalytic Reduction of NO_x with NH_3, *J. Am. Chem. Soc.*, 2024, **146**, 7605–7615.
40 K. Mlekodaj, J. Dedecek, V. Pashkova, E. Tabor, P. Klein, M. Urbanova, R. Karcz, P. Sazama, S. R. Whittleton, H. M. Thomas, A. V. Fishchuk and S. Sklenak, Al Organization in the SSZ-13 Zeolite. Al Distribution and Extraframework Sites of Divalent Cations, *J. Phys. Chem. C*, 2019, **123**, 7968–7987.
41 P. Wu, M. Yang, W. Zhang, S. Zeng, M. Gao, S. Xu, P. Tian and Z. Liu, Silicoaluminophosphate molecular sieve DNL-6: Synthesis with a novel template, N,N'-dimethyl-ethylenediamine, and its catalytic application, *Chin. J. Catal.*, 2018, **39**, 1511–1519.

 This journal is © the Partner Organisations 2026